Journal of Hazard Literacy
eISSN 3091-6402

Original Article
J. Hazard Lit. 2025;1(3):e16
https://doi.org/10.63737/jhl.25.0036

N-Acetyl-*L*-cysteine-grafted metal-organic framework for heavy metal removal from hazardous waste

Junmo Seong[1], Seonghwan Lee[1], Gyoung Hwa Jeong[2], Jaewoong Lim[3,4,*]
[1]Department of Chemistry, Ulsan National Institute of Science and Technology (UNIST), Ulsan, Korea
[2]Hydrogen Energy Technology Laboratory, Korea Institute of Energy Technology (KENTECH), Naju, Korea
[3]Department of Science Education, Ewha Womans University, Seoul, Korea
[4]Institute for Multiscale Matter and System (IMMS), Ewha Womans University, Seoul, Korea

Received: Nov 26, 2025
Revised: Dec 15, 2025
Accepted: Dec 18, 2025

***Corresponding author**
Jaewoong Lim
Department of Science Education, Ewha Womans University, Seoul, Korea
Tel: +82-2-3277-2641
E-mail: jaewoonglim@ewha.ac.kr

ORCID
Junmo Seong
https://orcid.org/0000-0003-0520-6246
Seonghwan Lee
https://orcid.org/0000-0003-0131-8830
Gyoung Hwa Jeong
https://orcid.org/0009-0003-7557-1203
Jaewoong Lim
https://orcid.org/0000-0002-4557-0870

Conflict of interest
No potential conflict of interest relevant to this article was reported.

Funding sources
This work was supported by the Ministry of Education of the Republic of Korea and the National Research Foundation of Korea (NRF-2024S1A5C3A03046593).

Abstract

Over the past century, industrial development has led to severe environmental problems, including the contamination of wastewater (such as from rivers and seas) with dissolved heavy metals (e.g., Pb^{2+} and Cd^{2+}), which pose serious health risks. To remove these heavy metals, heterogeneous solid-state adsorbents, such as metal-organic frameworks (MOFs) have attracted significant attention due to their porous extended structures, strong binding sites, ease of separation from water, and non-toxic, stable nature. In this work, we functionalized MOF-808 with *N*-acetyl-*L*-cysteine (AcC), which contains soft-base –SH groups capable of binding soft-acid metal ions (Pb^{2+} and Cd^{2+}), via grafting onto the Zr_6 metal nodes. Approximately 83% of the Zr_6 nodes in MOF-808 were successfully functionalized with AcC, yielding AcC@MOF-808. This modification enabled strong interactions between the AcC groups and heavy metals, consistent with hard-soft acid-base (HSAB) theory, while maintaining the crystallinity and availability of free –SH sites. As a result, AcC@MOF-808 demonstrated highly efficient capture of Pb^{2+} and Cd^{2+}, facilitated by the thiol groups along with the aliphatic and acetyl functionalities that enhance adsorption efficiency, as confirmed by crystallographic, spectroscopic, and microscopic analyses. The maximum adsorption capacities for Pb^{2+} and Cd^{2+} were 231 mg g^{-1} and 109 mg g^{-1}. AcC@MOF-808 achieved 99% removal of both Pb^{2+} and Cd^{2+} from 10 ppm trace metal solutions, exhibiting particularly rapid uptake (within seven minutes). The corresponding rate constant (k) values were 6.6×10^3 g mg^{-1} min^{-1} for Pb^{2+} and 1.1×10^3 g mg^{-1} min^{-1} for Cd^{2+}, and adsorption kinetics that followed a pseudo-second order model. Furthermore, AcC@MOF-808 showed high selectivity toward Pb^{2+} and Cd^{2+} over other divalent metal ions, including both alkali and transition metals, demonstrating its strong potential for heavy metal removal from real wastewater systems.

Keywords: metal-organic frameworks (MOFs), *N*-acetyl-*L*-cysteine, functional group grafting, heavy metal removal, hazardous waste

Introduction

Rapid industrial development has led to the release of wastewater containing toxic heavy metals,

Acknowledgements
This work was supported by the Ministry of Education of the Republic of Korea and the National Research Foundation of Korea (NRF- 2024S1A5C3A03046593).

Availability of data and material
The authors confirm that data supporting the findings of this study are available within the article.

Authors' contributions
Conceptualization: Seong J, Lim J.
Data curation: Seong J, Jeong GH.
Formal analysis: Seong J, Jeong GH.
Methodology: Seong J, Lim J.
Software: Seong J, Lee S.
Validation: Seong J, Lee S.
Investigation: Lim J.
Writing - original draft: Seong J, Lim J.
Writing - review & editing: Seong J, Lee S, Jeong GH, Lim J.

Ethics approval and consent to participate
Not applicable.

which can accumulate in the human body even at trace levels and cause severe health problems [1–3]. For example, lead (Pb) can interfere with bone biosynthesis, hinder erythrocyte formation by binding to enzymes in bloodstream, and damage multiple organs [4,5]. Cadmium (Cd), known for causing Itai-Itai disease, can induce kidney, nervous system, and skeletal disorders [6,7].

To remove such heavy metals from water, porous solid-state adsorbents such as zeolite, carbon materials, and functional polymers have been widely studied [8–12]. These materials often incorporate soft-base functional groups (e.g., –SH) that can strongly interact with soft-acid metal ions (i.e., heavy metal ions such as Pb^{2+} and Cd^{2+}) based on the hard-soft acid-base (HSAB) theory [11–13]. However, these traditional adsorbents suffer from several limitations, including poorly controlled pore sizes, challenges in including target functional groups, low adsorption capacities, weak binding affinities, and limited selectivity [14–16].

To overcome these challenges, metal-organic frameworks (MOFs) have emerged as highly tunable porous materials suitable for a wide range of applications, including heterogeneous catalysis, ionic conduction, sensors, gas storage, separation, and adsorption [17–26]. Their designable structures allow for precise control of pore size, surface area, and functionality, as well as high thermal and chemical stability [27–30]. Among them, Zr-based MOFs (e.g., UiO-66, UiO-67, MOF-808, NU-1000) have attracted particular interest because of their exceptional stability and their ability to introduce additional functional groups via Zr_6 metal nodes without compromising structural integrity [31–34]. For instance, sulfamic acid has been grafted onto MOF-808 (which has pore sizes of 11.8 Å and 18.4 Å) through the six unsaturated coordination sites of the Zr_6 nodes, enhancing acidity and improving proton conductivity under humidity conditions [35].

In this work, we first grafted *N*-acetyl-*L*-cysteine (AcC) onto MOF-808 ($Zr_6O_4(OH)_4(BTC)_2X_6$, where H_3BTC=1,3,5-bezenetricarboxylic acid and X^- represents formate or OH^-) through ligand exchange at the X^- sites. AcC contains thiol (–SH) groups that serve as active sites for capturing soft-acid metal ions (Pb^{2+} and Cd^{2+}), derived from the *L*-cysteine (Cys) moiety, which is widely used in medicines and dietary supplements (Fig. 1). Its aliphatic fragment improves solubility in methanol, facilitating incorporation into the Zr_6 nodes. This resulting AcC@MOF-808 contained five AcC ligands per Zr_6 cluster (corresponding to 83% of the available sites) and retained free –

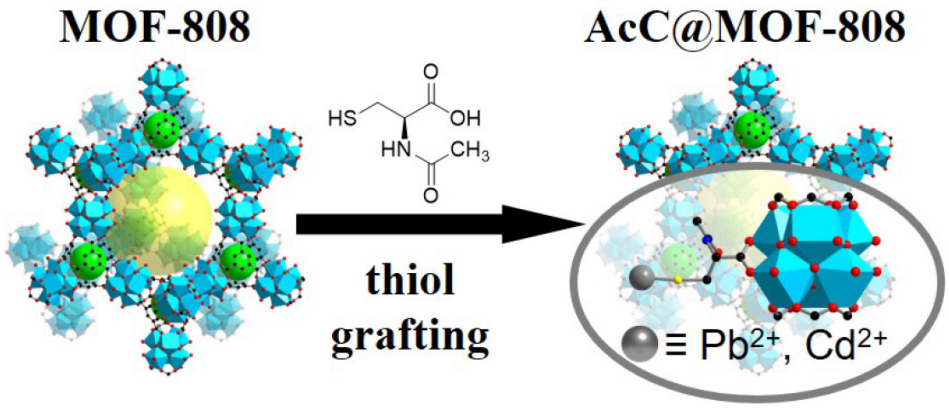

Fig. 1. Schematic representation of AcC@MOF-808 synthesis and heavy metal (Pb^{2+} and Cd^{2+}) capture via thiol groups from grafted *N*-acetyl-*L*-cysteine. The inset shows a structural model of heavy metal coordination to the Zr_6 cluster. The green and yellow spheres represent 11.8 Å and 18.4 Å, respectively. 1 Zr node is represented by the blue polyhedral, consisting of the red, black, blue, and yellow spheres representing oxygen, carbon, nitrogen, and sulfur, respectively. AcC, *N*-acetyl-*L*-cysteine; MOFs, metal-organic frameworks.

SH groups after modification.

Through these accessible thiol groups, together with the aliphatic and acetyl functionalities introduced within the MOF pores, AcC@MOF-808 effectively adsorbed Pb^{2+} and Cd^{2+} while maintaining its crystallinity and morphology, confirming its stability as a heterogeneous solid-state adsorbent. The removal efficiencies for Pb^{2+} and Cd^{2+} were both 99%, significantly higher than those for other divalent alkali and transition metal ions (Mg^{2+}, Ca^{2+}, and Zn^{2+}). Notably, AcC@MOF-808 removed 99% for Pb^{2+} within seven minutes. Owing to this rapid adsorption behavior, kinetic studies revealed that the process followed a pseudo-second order model, with rate constant (k) values of 6.6×10^{3} g mg^{-1} min^{-1} and 1.1×10^{3} g mg^{-1} min^{-1} for Pb^{2+} and Cd^{2+}, respectively, which are competitive with those of other thiol-based adsorbents. The maximum adsorption capacities were 231 mg g^{-1} for Pb^{2+} and 109 mg g^{-1} for Cd^{2+}.

This work demonstrates the successful incorporation of an eco-friendly amino acid derivative (AcC) into MOF-808, resulting in a stable, functionalized framework capable of selectively and efficiently removing heavy metals from aqueous systems. Our results highlight the potential of amino acid-modified MOFs as robust and sustainable adsorbents for real-world water purification applications.

Methods

Materials

Commercially available reagents were purchased in high purity and used without further purification. $ZrOCl_2{\cdot}8H_2O$ (99.5%), $Pb(NO_3)_2$ (99.999%), $Cd(NO_3)_2{\cdot}4H_2O$ (99.997%), 1,3,5-benezene tricarboxylic acid (95%), and AcC (99%) were purchased from Sigma-Aldrich. Formic acid (96%) was purchased from Daejung Chemicals & Metals. *N*,*N*-dimethylformamide (DMF; 99.5%) and methanol (99.8%) were purchased from Junsei Chemical (Tokyo, Japan).

General procedures

Powder X-ray diffraction (PXRD) patterns were recorded on a Rigaku D/max-2400 X-ray powder diffractometer (Tokyo, Japan) using Cu-K_α (λ=1.5405 Å) radiation. Fourier transform infrared (FTIR) spectroscopy was recorded as Attenuated Total Reflectance method using a NICOLET iS 10 FT-IR spectrophotometer. ^{1}H nuclear magnetic resonance (NMR) spectra were measured on Bruker model AVANCE III HD, 400 MHz NMR spectrometer. Scanning electron microscopy (SEM) was performed using a FEI model Nova Nano230. High-resolution transmission electron microscopy (HR-TEM) and energy dispersive spectroscopy (EDS) elemental mapping were performed using a JEOL model JEM-2100F (Cs corrector). Inductively coupled plasma mass spectroscopy (ICP-MS) and inductively coupled plasma optical emission spectroscopy (ICP-OES) data was gathered from Perkin Elmer model ELAN DRC-II and Varian model 700-ES. X-ray photoelectron spectroscopy (XPS) was performed using a Thermo Scientific instrument and K-alpha surface analysis. N_2 sorption isotherms were measured using a BELSORP-max (BEL Japan, Tokyo, Japan) adsorption system, employing a standard volumetric technique up to saturation pressure N_2 sorption isotherms were monitored at 77 K.

Synthesis of MOF-808

MOF-808 was synthesized following a slightly modified literature procedure [35]. In a 100-mL vial, $ZrOCl_2{\cdot}8H_2O$ (483 mg, 1.50 mmol) and 1,3,5-benezene tricarboxylic acid (H_3BTC; 315 mg, 1.50 mmol) were dissolved in 15.0 mL of DMF along with 15.0 mL of formic acid. The resulting

https://doi.org/10.63737/jhl.25.0036

solution was heated in an oven at 100℃ for 18 hours. After cooling to room temperature, the white precipitate was collected and washed three times with fresh DMF and four times with methanol (MeOH) by centrifugation. The product was then dried under vacuum at 60℃ overnight. The PXRD pattern matched the reported simulated pattern (Fig. 2).

Synthesis of AcC@MOF-808

In a 20-mL vial, 100 mg of MOF-808 were dispersed in 5.00 mL of MeOH, followed by the addition of 5.00 mL of 0.300 M AcC in MeOH. After soaking for 12 hours at room temperature, the product was collected by centrifugation and washed three times with fresh MeOH. The washed sample was dried under vacuum at 60℃ overnight to remove residual solvent. The crystallinity of AcC@MOF-808 was maintained throughout all the experimental procedures, as confirmed by PXRD (Figs. 2 and 3). The number of AcC integrated within MOF-808 was calculated using ^{1}H NMR spectroscopy of the digested sample (2.00 mg of AcC@MOF-808 dissolved in a mixed solvent of 0.600 mL DMSO-d_6 and 50.0 μL of D_2SO_4) based on the integration of the resonance corresponding to H_3BTC and AcC (Supplementary Fig. S1). The morphology and particle size were confirmed by SEM (Supplementary Fig. S2).

Heavy metal adsorption isotherm

To investigate the adsorption behavior of heavy metal ions, Langmuir isotherm model was employed (Eq. 1) [36,37]. In a 20-mL vial, 10.0 mL of $Pb(NO_3)_2$ or $Cd(NO_3)_2$ aqueous solutions at varying initial concentrations (10, 20, 50, 100, 250, 500, 1,000, and 2,000 ppm) were added to 10.0 mg of AcC@MOF-808. After stirring for six hours at room temperature, the mixtures were vacuum filtered, and the filtrates were collected to determine the remaining concentrations of Pb^{2+} (or Cd^{2+}) using ICP-OES.

To confirm that heavy metals were adsorbed onto AcC@MOF-808, the sample obtained from the 2,000 ppm adsorption experimental was analyzed. The crystallinity of AcC@MOF-808 was maintained after both Pb^{2+} and Cd^{2+} adsorption (Fig. 3). The successful coordination of heavy metals within the framework was further supported by XPS and TEM coupled with energy-

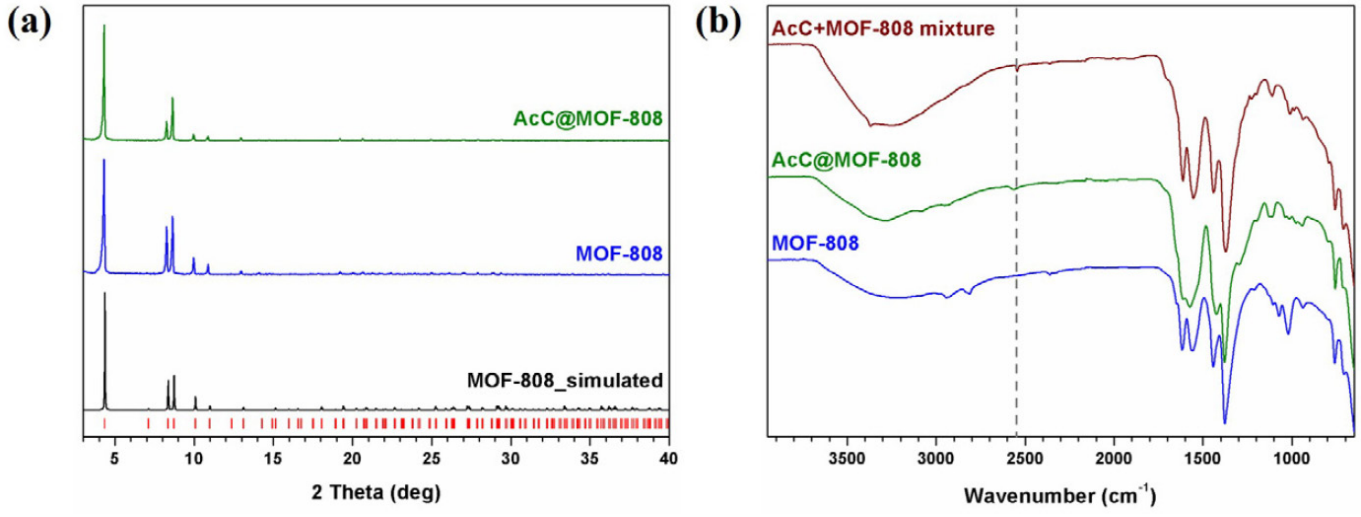

Fig. 2. Comparisons of (a) PXRD patterns of MOF-808 and AcC@MOF-808 and (b) FTIR spectra of MOF-808, AcC@MOF-808, and physical mixture of AcC and MOF-808. Gray dashed line (2,563 cm^{-1}) indicate S–H stretching bonding. PXRD, powder X-ray diffraction; MOFs, metal-organic frameworks; AcC, *N*-acetyl-*L*-cysteine; FTIR, Fourier transform infrared.

https://doi.org/10.63737/jhl.25.0036

dispersive X-ray spectroscopy (TEM-EDS) (Figs. 3 and 4)

The adsorption capacities and removal efficiencies are presented in Fig. 5a, while the Langmuir model fitting used to determine the maximum adsorption capacities is shown in Supplementary Fig. S4. The experimental data fit the Langmuir model well, with correlation coefficients (R^2) of 0.999 for both Pb^{2+} and Cd^{2+}, allowing reliable estimation of the maximum adsorption capacities (q_{max}).

The linearized form of the Langmuir isotherm equation is given as:

$$\frac{C_e}{q_e} = \frac{1}{q_{max} K_L} + \frac{C_e}{q_{max}} \quad \text{(Eq. 1)}$$

where C_e (mg L^{-1}) and q_e (mg g^{-1}) represent the equilibrium concentration and adsorption amount of M^{2+} (M=Pb and Cd), respectively; q_{max} (mg g^{-1}) is the maximum adsorption capacity, and K_L (L mg^{-1}) is the Langmuir constant.

Adsorption kinetics study

To analyze the adsorption kinetics, the pseudo-second-order kinetic model was applied (Eq. 2) [36,37]. In a 20-mL vial, 10.0 mL of $Pb(NO_3)_2$ or $Cd(NO_3)_2$ aqueous solutions (10 ppm) were added to 10.0 mg of AcC@MOF-808. The mixtures were stirred for different time intervals ranging from three to 360 minutes at room temperature, then vacuum filtered, and the filtrates were collected to determine the remaining concentrations of Pb^{2+} and Cd^{2+} using ICP-MS.

The experimental kinetic data are presented in Fig. 5b, and the corresponding pseudo-second-order model fittings are shown in Supplementary Fig. S5 (Eq. 2). The data fitted the pseudo-second-order model well, with R^2=0.999 for both Pb^{2+} and Cd^{2+}, allowing reliable estimation of rate constant (k_2).

The linearized form of the pseudo-second-order equation is given as:

$$\frac{t}{q_t} = \frac{t}{q_e} + \frac{1}{k_2 q_e^2} \quad \text{(Eq. 2)}$$

where q_t (mg g^{-1}) and q_e (mg g^{-1}) represent the adsorption amounts of M^{2+} (M=Pb and Cd) at any time t and at equilibrium, respectively; k_2 (g mg^{-1} min^{-1}) is the rate constant.

Results

To graft thiol groups onto a heterogeneous solid-state adsorbent for heavy metal removal, we employed MOFs as scaffolds [14–16]. Among them, Zr-based MOFs were selected because of their exceptional stability, which arises from the strong coordination between Zr^{4+} (a hard acid) and carboxylate ligands (hard bases) [31,32]. In particular, MOF-808 was chosen for this study because its Zr_6 nodes contain up to six coordination sites occupied by formate ligands that can be exchanged with hydroxyl groups, allowing further functionalization with organic linkers such as amino acids or sulfamic acid [35]. In addition, MOF-808 possesses large pore sizes (11.8 Å and 18.4 Å), providing sufficient space for grafting functional molecules and accommodating heavy metal ions (Fig. 1) [35].

MOF-808 was first synthesized following a modified literature procedure using $ZrOCl_2 \cdot 8H_2O$, 1,3,5-bezenetricarboxylic acid (H_3BTC), and formic acid in DMF at 100℃ for 18 hours (see

https://doi.org/10.63737/jhl.25.0036

Methods for details) [35]. This resulting product exhibited 400–600 nm octahedral particles without impurities, as confirmed by PXRD and SEM analyses (Figs. 2 and Supplementary Table S1).

Next, to introduce soft-base functional groups, AcC was selected because it contains both carboxylic acid groups (capable of coordinating to the Zr_6 nodes) and thiol groups (for binding soft-acid metal ions such as Pb^{2+} and Cd^{2+}) (Fig. 1). The aliphatic moiety of AcC also enhances its solubility in methanol, facilitating the grafting process. Prior to functionalization, formate ligands on MOF-808 were exchanged with hydroxyl groups through methanol treatment to create accessible coordination sites [35]. Subsequently, MOF-808 was immersed in a methanolic solution of AcC and stirred for 12 hours, yielding AcC@MOF-808 after washing to remove unreacted AcC (see Methods for details).

PXRD and SEM analyses confirmed that AcC@MOF-808 retained the crystallinity and morphology of the parent MOF, with no observable impurities (Figs. 2 and Supplementary Table S1) To determine the number of AcC molecules coordinated to each Zr_6 node, digestion NMR spectroscopy was performed, revealing that five AcC molecules were grafted per Zr_6 node, corresponding to 83% of the available coordination sites (Supplementary Fig. S2). The N_2 adsorption isotherms (77 K) showed a noticeable decrease in adsorption capacity for AcC@MOF-808 relative to pristine MOF-808, consistent with the successful incorporation of AcC within the framework (Supplementary Fig. S3). In addition, the Brunauer-Emmett-Teller (BET) surface areas and pore volumes decreased after AcC grafting, consistent with the N_2 adsorption isotherm results, indicating that AcC occupies the internal pore volume of MOF-808 (Table S1).

The presence of free thiol (–SH) groups after functionalization of MOF-808 to AcC@MOF-808 was confirmed by FTIR spectroscopy, which showed a distinct –SH stretching band from AcC at 2,563 cm^{-1}, also observed in the physical mixture of MOF-808 and AcC for comparison (Fig. 2).

Having established the successful incorporation of AcC and the presence of accessible thiol sites, we next evaluated the heavy metal binding performance of AcC@MOF-808 toward Pb^{2+} and Cd^{2+} ions as a model system for wastewater purification. As a point of comparison, it has been reported that pristine MOF-808, which lacks thiol groups, does not adsorb Pb^{2+} or Cd^{2+} [38]. To determine the maximum adsorption capacity for heavy metal ions, 1,000 ppm aqueous solutions of $Pb(NO_3)_2$ and $Cd(NO_3)_2$ were prepared. Then, 10 mg of AcC@MOF-808 was added to each metal solution, corresponding to 100 equivalents of metal ions per MOF. The mixtures were stirred for six hours to ensure saturation of metal uptakes. After soaking, we measured ICP-OES after filtration to check Pb and Cd amounts for MOF precipitants (Supplementary Fig. S4). To calculate the potential maximum uptake of AcC@MOF-808, Langmuir isotherm model was performed, and we found that AcC@MOF-808 were able to uptake maximum 231 mg g^{1} for Pb^{2+} and 109 mg g^{-1} for Cd^{2+} (Supplementary Fig. S4) [36,37]. After soaking in 1,000 ppm heavy metal solutions, AcC@MOF-808 were both maintain their crystallinity in Pb^{2+} and Cd^{2+} solutions, which exhibited the potential for sustainable solid-state adsorbents (Fig. 3). In addition, after exposure to Cd^{2+} solution, AcC@MOF-808 maintained their thiol group 163 eV and contained Cd^{2+} at 405 eV and 411 eV by confirming XPS results (Fig. 3).

To confirm the metal ion adsorption occurred not only on the surface but also within the internal pores of AcC@MOF-808, TEM coupled with energy-dispersive X-ray spectroscopy (EDS) was performed on AcC@MOF-808 samples after Pb^{2+} and Cd^{2+} adsorption (Fig. 4). The TEM-EDS elemental mapping of both Pb- and Cd-loaded AcC@MOF-808 revealed homogeneous distributions of Pb and Cd throughout the particles. The uniform overlap of Pb/Cd with Zr and S signals indicates that Pb^{2+} and Cd^{2+} ions were bound to the thiol groups uniformly across the entire framework, demonstrating efficient diffusion and adsorption

https://doi.org/10.63737/jhl.25.0036

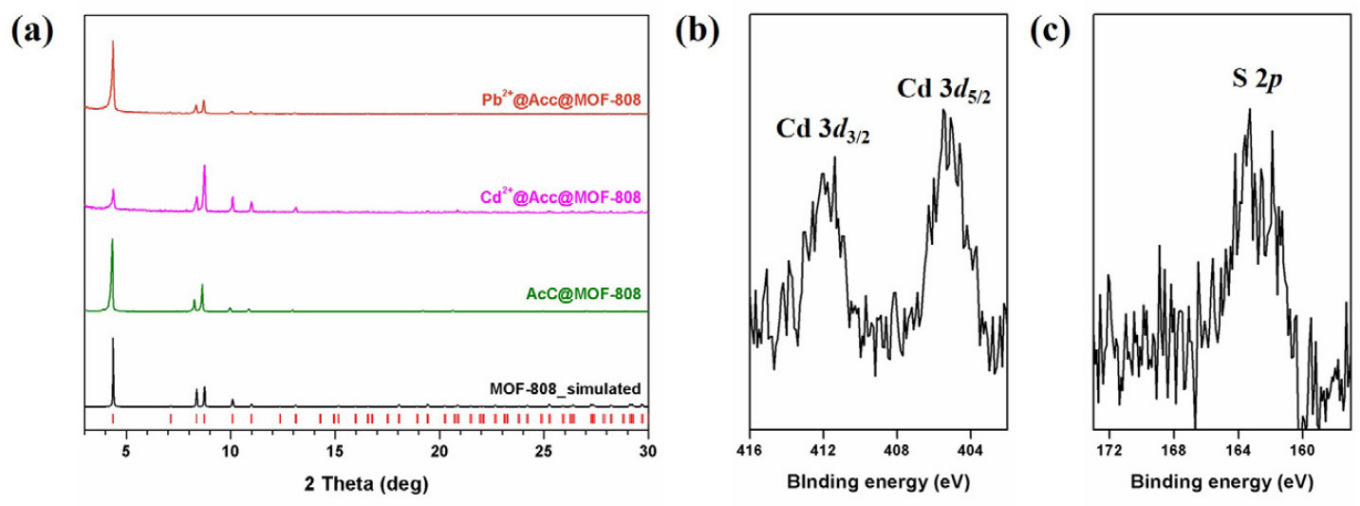

Fig. 3. (a) PXRD patterns of AcC@MOF-808 after heavy metal adsorption (orange: $Pb(NO_3)_2$ and pink: $Cd(NO_3)_2$). XPS spectra of AcC@MOF-808 after $Cd(NO_3)_2$ adsorption for the **(b) Cd 3d and (c) S 2p regions.** PXRD, powder X-ray diffraction; AcC, *N*-acetyl-*L*-cysteine; MOFs, metal-organic frameworks; XPS, X-ray photoelectron spectroscopy.

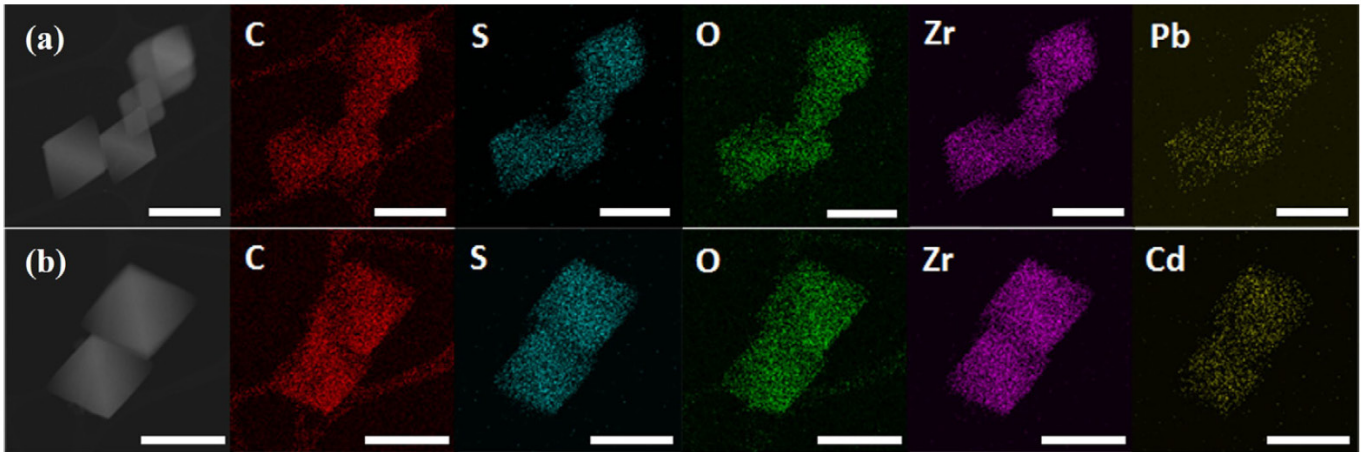

Fig. 4. TEM-EDS elemental mapping of AcC@MOF-808 after (a) $Pb(NO_3)_2$ and (b) $Cd(NO_3)_2$ adsorption, indicating the homogeneous distribution of AcC and adsorbed heavy metal ions (Pb^{2+} and Cd^{2+}) throughout the particles. Scale bars represent 500 nm. TEM-EDS, transmission electron microscopy coupled with energy-dispersive X-ray spectroscopy; AcC, *N*-acetyl-*L*-cysteine; MOFs, metal-organic frameworks.

throughout the MOF structure (Fig. 4).

To evaluate the removal efficiency of AcC@MOF-808 under realistic conditions, we tested its performance for the adsorption of trace concentrations of heavy metal ions, as typically found in contaminated drinking water systems [1–3]. For this purpose, 10 ppm aqueous solutions of Pb^{2+} and Cd^{2+} were prepared and treated with AcC@MOF-808 as a solid-state adsorbent (Fig. 5). AcC@MOF-808 rapidly removed Pb^{2+}, achieving 97% removal within three minutes and 99% within seven minutes. Cd^{2+} adsorption was slightly slower, with 95% removal at 15 minutes and 99% after three hours, demonstrating the high adsorption efficiency of AcC@MOF-808 even at low metal concentrations.

To further investigate the adsorption mechanism, kinetic studies were carried out using the pseudo-second order model and the experimental data fitted this model well, with correlation coefficients (R^2) of 0.999 for both Pb^{2+} and Cd^{2+} (Figs. 5b and Supplementary Fig S5) [36,37].

https://doi.org/10.63737/jhl.25.0036

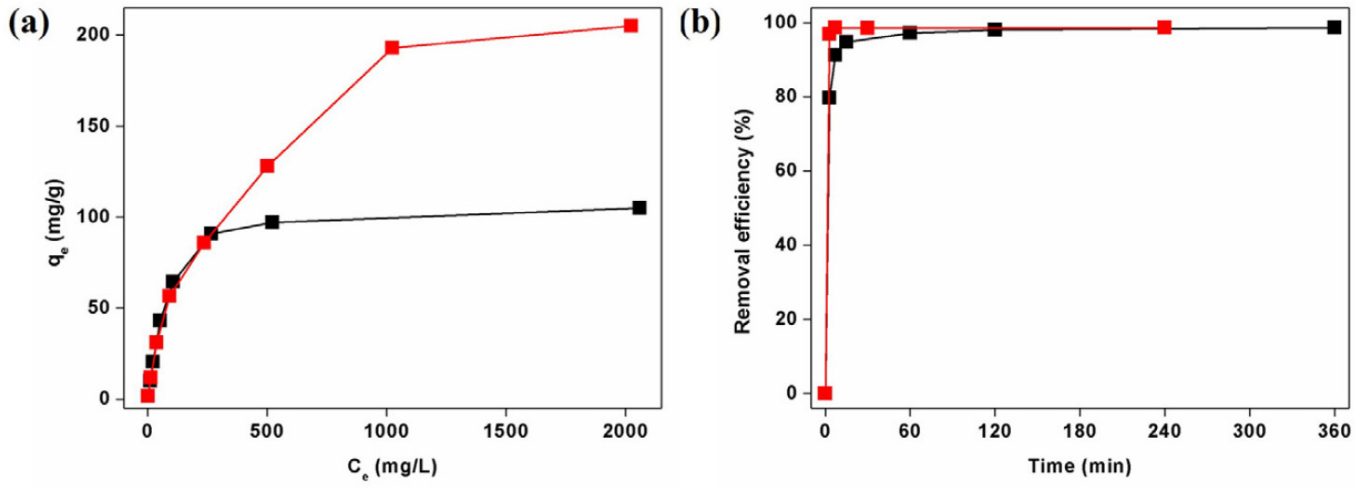

Fig. 5. Heavy metal adsorption performance of AcC@MOF-808. (a) Adsorption capacities of AcC@MOF-808 for heavy metal ions Pb^{2+} (red) and Cd^{2+} (black) across different initial concentrations. (b) Removal kinetics of Pb^{2+} (red) and Cd^{2+} (black) by AcC@MOF-808 in 10 ppm trace concentration aqueous solutions. AcC, *N*-acetyl-*L*-cysteine; MOFs, metal-organic frameworks.

Interestingly, we found that the rate constants (k) for both metal ions exhibited relatively fast adsorption kinetics compared to other MOF-based adsorbents [16]. This enhanced rate is attributed to the flexible aliphatic fragment of AcC, which allows greater molecular mobility and increased the probability of thiol–metal binding. The rate constant for Pb^{2+} adsorption was calculated as 6.6×10^3 g mg^{-1} min^{-1}, comparable to previously reported thiol-functionalized adsorbents with aliphatic moieties, such as SiO_2–Al_2O_3–Silane-SH (k = 3.7×10^3 g mg^{-1} min^{-1}) [39]. Similarly, the k value for Cd^{2+} adsorption was 1.1×10^3 g mg^{-1} min^{-1}, in line with reported values for other thiol-based Cd^{2+} adsorbents (e.g., SiO_2–Al_2O_3–Silane-SH, k = 4.7×10^3 g mg^{-1} min^{-1}) [39].

In addition, these adsorption rates are significantly faster than those reported for thiol-based amino acid-grafted MOF-808 materials (MOF-808@Msc and MOF-808@Cys), which require more than 200 minutes for heavy metal uptake [38]. Notably, AcC@MOF-808 achieves Pb^{2+} adsorption approximately 20 times faster while also exhibiting higher capacities than these materials (MOF-808@Cys: 175 mg g^{-1} for Pb^{2+} and 40 mg g^{-1} for Cd^{2+}; MOF-808@Msc is unstable under acidic conditions), owing to the presence of the aliphatic fragment and acetyl groups in AcC [36]. These results confirm that AcC@MOF-808 is a highly effective adsorbent for heavy metal ions and has strong potential for practical water purification applications.

AcC@MOF-808 exhibited highly efficient adsorption of Pb^{2+} and Cd^{2+} ions. To further evaluate its selectivity toward these soft-acid heavy metal ions, competitive adsorption experiments were performed using other divalent metal ions commonly found in real water systems, including Zn^{2+}, Ca^{2+}, and Mg^{2+} [14–16]. Under the same conditions used for Pb^{2+} and Cd^{2+} adsorption, 10 ppm aqueous solutions of $Zn(NO_3)_2$, $Ca(NO_3)_2$, and $Mg(NO_3)_2$ were prepared and tested with AcC@MOF-808 as the adsorbent. The removal efficiencies were 19% for Zn^{2+}, 6% for Ca^{2+}, and 2% for Mg^{2+} (Fig. 6).

These results indicate that AcC@MOF-808 shows strong selectivity for soft-acid metal ions (Pb^{2+} and Cd^{2+}) over hard-acid ions (Ca^{2+} and Mg^{2+}) (Fig. 6). The moderate adsorption of Zn^{2+} can be attributed to its intermediate acid-base character, which allows partial interaction with the thiol groups of AcC, but still much weaker than that observed for Pb^{2+} and Cd^{2+} (Fig. 6). Overall, the strong preference for Pb^{2+} and Cd^{2+} confirms that the thiol-functionalized MOF framework

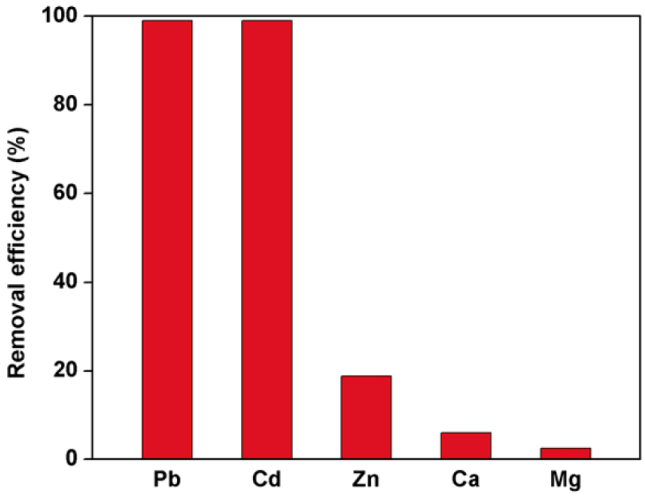

Fig. 6. Removal efficiencies of AcC@MOF-808 for various divalent metal ions, demonstrating highly selective removal of heavy metal ions (Pb^{2+} and Cd^{2+}). AcC, *N*-acetyl-*L*-cysteine; MOFs, metal-organic frameworks.

acts as an effective and selective solid-state adsorbent for soft-acid heavy metal ions.

In conclusion, we successfully demonstrated the grafting of AcC, which contains thiol functional groups with aliphatic fragments and acetyl groups, onto MOF-808 to achieve selective and rapid adsorption of heavy metal ions (Pb^{2+} and Cd^{2+}) over other divalent ions (Zn^{2+}, Ca^{2+}, and Mg^{2+}) in aqueous systems. AcC was coordinated to 83% of the available sites of Zr_6 clusters through carboxylate linkages, while the resulting AcC@MOF-808 retained its crystallinity, morphology, and porosity, enabling a high density of accessible thiol sites within the framework. Owing to the high grafting efficiency, the maximum adsorption capacities for Pb^{2+} and Cd^{2+} reached 231 mg g^{-1} and 109 mg g^{-1}, respectively. Spectroscopic and microscopic analyses confirmed that heavy metal ions were uniformly adsorbed throughout the framework without structural degradation. At trace concentrations (10 ppm), AcC@MOF-808 achieved remarkable removal efficiencies of 99% for Pb^{2+}, including rapid uptake within the first seven minutes, and Cd^{2+}, while showing minimal uptake for competing ions (Zn^{2+}, 19%; Ca^{2+}, 6%; Mg^{2+}, 2%), consistent with the HSAB principle. The adsorption kinetics followed a pseudo-second order model, indicative of a chemisorption mechanism, with rate constants (k) of 6.6×10^3 g mg^{-1} min^{-1} for Pb^{2+} and 1.1×10^3 g mg^{-1} min^{-1} for Cd^{2+}. These results demonstrate that AcC-functionalized MOFs serve as robust, selective, and eco-friendly solid-state adsorbents for efficient heavy metal removal from aqueous environments.

Looking forward, this study can be extended by incorporating other amino acid-derived ligands with diverse functional groups to fine-tune the pore environment and metal ion selectivity of MOFs. Such eco-friendly frameworks could also serve as promising candidates for catalysis or adsorption of larger hazardous organic molecules. Further optimization toward enhanced reusability, stability, and scalable synthesis would accelerate the practical application of amino acid-functionalized MOFs in real wastewater purification and environmental remediation systems.

Supplementary Materials

Supplementary materials are only available online from: https://doi.org/10.63737/jhl.25.0036

References

1. Uliana AA, Bui NT, Kamcev J, Taylor MK, Urban JJ, Long JR. Ion-capture electrodialysis using multifunctional adsorptive membranes. Science 2021;372:296-299. https://doi.org/10.1126/science.abf5991
2. Nakahata M, Sumiya A, Ikemoto Y, Nakamura T, Dudin A, Schwieger J, et al. Hyperconfined bio-inspired polymers in integrative flow-through systems for highly selective removal of heavy metal ions. Nat Commun 2024;15:5824. https://doi.org/10.1038/s41467-024-49869-8
3. Bolisetty S, Mezzenga R. Amyloid–carbon hybrid membranes for universal water purification. Nat Nanotechnol 2016;11:365-371. https://doi.org/10.1038/nnano.2015.310
4. Collin MS, Venkatraman SK, Vijayakumar N, Kanimozhi V, Arbaaz SM, Stacey RGS, et al. Bioaccumulation of lead (Pb) and its effects on human: a review. J Hazard Mater Adv 2022;7:100094. https://doi.org/10.1016/j.hazadv.2022.100094
5. Yu YL, Yang WY, Hara A, Asayama K, Roels HA, Nawrot TS, et al. Public and occupational health risks related to lead exposure updated according to present-day blood lead levels. Hypertens Res 2023;46:395-407. https://doi.org/10.1038/s41440-022-01069-x
6. Rasin P, Ashwathi AV, Basheer SM, Haribabu J, Santibanez JF, Garrote CA, et al. Exposure to cadmium and its impacts on human health: a short review. J Hazard Mater Adv 2025;17:100608. https://doi.org/10.1016/j.hazadv.2025.100608
7. Zhao D, Lin GB, Liu C, Juhasz AL, Ma LQ. Health risk assessment of dietary cadmium exposure based on cadmium bioavailability in food: opportunities and challenges. J Hazard Mater 2025;488:137359. https://doi.org/10.1016/j.jhazmat.2025.137359
8. Finish N, Ramos P, Borojovich EJC, Zeiri O, Amar Y, Gottlieb M. Zeolite performance in removal of multicomponent heavy metal contamination from wastewater. J Hazard Mater 2023;457:131784. https://doi.org/10.1016/j.jhazmat.2023.131784
9. Wang B, Lan J, Bo C, Gong B, Ou J. Adsorption of heavy metal onto biomass-derived activated carbon: review. RSC Adv 2023;13:4275-4302. https://doi.org/10.1039/d2ra07911a
10. Zhang Y, Vallin JR, Sahoo JK, Gao F, Boudouris BW, Webber MJ, et al. High-affinity detection and capture of heavy metal contaminants using block polymer composite membranes. ACS Cent Sci 2018;4:1697-1707. https://doi.org/10.1021/acscentsci.8b00690
11. Zhang W, An Y, Li S, Liu Z, Chen Z, Ren Y, et al. Enhanced heavy metal removal from an aqueous environment using an eco-friendly and sustainable adsorbent. Sci Rep 2020;10:16453. https://doi.org/10.1038/s41598-020-73570-7
12. Gou X, Li Y, Ahmad Z, Zhu X, Chen J. Thiolated polyethyleneimine-based polymer sponge for selective removal of Hg^{2+} from aqueous solution. ACS Omega 2021;6:31955-31963. https://doi.org/10.1021/acsomega.1c04729
13. Pearson RG. Hard and soft acids and bases. J Am Chem Soc 1963;85:3533-3539. https://doi.org/10.1021/ja00905a001
14. Li J, Lin G, Liang H, Wang S, Hu T, Li S, et al. Recent advances in the synthesis of MOF-based composites for heavy-metal ion adsorption. Coord Chem Rev 2025;545:217010. https://doi.org/10.1016/j.ccr.2025.217010
15. Zhang X, Zhai Z, Feng X, Hou H, Zhang Y. Recent advances of metal–organic framework for heavy metal ions adsorption. Langmuir 2024;40:17868-17888. https://doi.org/10.1021/acs.langmuir.4c01757
16. Lam ITY, Choi SJ, Lu D, Kim Y. Functionalized metal–organic frameworks for heavy metal ion removal from water. Nanoscale 2023;15:10189-10205. https://doi.org/10.1039/

D3NR02250A
17. Canossa S, Ji Z, Gropp C, Rong Z, Ploetz E, Wuttke S, et al. System of sequences in multivariate reticular structures. Nat Rev Mater 2023;8:331-340. https://doi.org/10.1038/s41578-022-00482-5
18. Nguyen HL, Darù A, Chheda S, Alawadhi AH, Neumann SE, Wang L, et al. Pinpointing the onset of water harvesting in reticular frameworks from structure. ACS Cent Sci 2025;11:665-671. https://doi.org/10.1021/acscentsci.4c01878
19. Park J, Lim J, Moon HR. Strategic engineering of structural complexity in metal–organic frameworks. Trends Chem 2025;7:590-602. https://doi.org/10.1016/j.trechm.2025.08.006
20. Barsoum ML, Fahy KM, Morris W, Dravid VP, Hernandez B, Farha OK. The road ahead for metal–organic frameworks: current landscape, challenges and future prospects. ACS Nano 2025;19:13-20. https://doi.org/10.1021/acsnano.4c14744
21. Lim J, Lee S, Ha H, Seong J, Jeong S, Kim M, et al. Amine-tagged fragmented ligand installation for covalent modification of MOF-74. Angew Chem Int Ed 2021;60:9296-9300. https://doi.org/10.1002/anie.202100456
22. Jin E, Bon V, Das S, Wonanke ADD, Etter M, Karlsen MA, et al. Engineering photoswitching dynamics in 3D photochromic metal–organic frameworks through a metal–organic polyhedron design. J Am Chem Soc 2025;147:8568-8577. https://doi.org/10.1021/jacs.4c17203
23. Sharma A, Lim J, Lah MS. Strategies for designing metal–organic frameworks with superprotonic conductivity. Coord Chem Rev 2023;479:214995. https://doi.org/10.1016/j.ccr.2022.214995
24. Jang W, Yoo H, Shin D, Noh S, Kim JY. Colorimetric identification of colorless acid vapors using a metal-organic framework-based sensor. Nat Commun 2025;16:385. https://doi.org/10.1038/s41467-024-55774-x
25. Han Y, Wang L, Zhang Y, Chen B. Metal–organic frameworks for one-step ethylene purification from multi-component hydrocarbon mixtures. Coord Chem Rev 2025;523:216291. https://doi.org/10.1016/j.ccr.2024.216291
26. Lim J, Lee S, Sharma A, Seong J, Baek SB, Lah MS. Ligand functionalization of defect-engineered Ni-MOF-74. RSC Adv 2022;12:31451-31455. https://doi.org/10.1039/d2ra06587h
27. Terrones GG, Huang SP, Rivera MP, Yue S, Hernandez A, Kulik HJ. Metal–organic framework stability in water and harsh environments from data-driven models trained on the diverse WS24 data set. J Am Chem Soc 2024;146:20333-20348. https://doi.org/10.1021/jacs.4c05879
28. Ding M, Cai X, Jiang HL. Improving MOF stability: approaches and applications. Chem Sci 2019;10:10209-10230. https://doi.org/10.1039/C9SC03916C
29. Lv XL, Yuan S, Xie LH, Darke HF, Chen Y, He T, et al. Ligand rigidification for enhancing the stability of metal–organic frameworks. J Am Chem Soc 2019;141:10283-10293. https://doi.org/10.1021/jacs.9b02947
30. Lim J, Park KC, Thaggard GC, Liu Y, Kankanamalage BKPM, Toler DJ, et al. Friends or foes: fundamental principles of Th-organic scaffold chemistry using Zr-analogs as a guide. J Am Chem Soc 2024;146:12155-12166. https://doi.org/10.1021/jacs.4c02327
31. Daliran S, Oveisi AR, Kung CW, Sen U, Dhakshinamoorthy A, Chuang CH, et al. Defect-enabling zirconium-based metal–organic frameworks for energy and environmental remediation applications. Chem Soc Rev 2024;53:6244-6294. https://doi.org/10.1039/d3cs01057k

32. Chattopadhyay K, Mandal M, Maiti DK. A review on zirconium-based metal–organic frameworks: synthetic approaches and biomedical applications. Mater Adv 2024;5:51-67. https://doi.org/10.1039/D3MA00735A
33. Chen OIF, Liu CH, Wang K, Borrego-Marin E, Li H, Alawadhi AH, et al. Water-enhanced direct air capture of carbon dioxide in metal–organic frameworks. J Am Chem Soc 2024;146:2835-2844. https://doi.org/10.1021/jacs.3c14125
34. Haimerl J, Thaggard GC, Kankanamalage BKPM, Bühler R, Lim J, Park KC, et al. Shifting gears: photochromic metal–organic frameworks with stimulus-adaptable performance. J Am Chem Soc 2025;147:19918-19930. https://doi.org/10.1021/jacs.5c04466
35. Sharma A, Lim J, Jeong S, Won S, Seong J, Lee S, et al. Superprotonic conductivity of MOF-808 achieved by controlling the binding mode of grafted sulfamate. Angew Chem Int Ed 2021;60:14334-14338. https://doi.org/10.1002/anie.202103191
36. Yang P, Shu Y, Zhuang Q, Li Y, Gu J. Metal–organic frameworks bearing dense alkyl thiol for the efficient degradation and concomitant removal of toxic Cr(VI). Langmuir 2019;35:16226-16233. https://doi.org/10.1021/acs.langmuir.9b03057
37. Zha X, Lu Z, Liu J, Lu S, Wang Y. Selective Co(II) adsorption using hollow ZIF-8 nanostructures with embedded Fe_3O_4 nanoparticles. ACS Appl Nano Mater 2023;6:23630-23638. https://doi.org/10.1021/acsanm.3c05052
38. Valverde A, Tovar GI, Rio-López NA, Torres D, Rosales M, Wuttke S, et al. Designing metal-chelator-like traps by encoding amino acids in zirconium-based metal–organic frameworks. Chem Mater 2022;34:9666-9684. https://doi.org/10.1021/acs.chemmater.2c02431
39. Rozyyev V, Gao F, Liu Y, Shevate R, Pathak R, Mane AU, et al. Thiol-functionalized adsorbents through atomic layer deposition and vapor-phase silanization for heavy metal ion removal. ACS Appl Mater Interfaces 2024;16:34030-34041. https://doi.org/10.1021/acsami.4c03935